

The Starburst in the Central Kiloparsec of Markarian 231

G. B. Taylor, C. S. Silver, J. S. Ulvestad, & C. L. Carilli;
 gtaylor,csilver,julvestad,ccarilli@nrao.edu
 National Radio Astronomy Observatory,
 P.O. Box O, Socorro, NM 87801, USA

ABSTRACT

We present VLBA observations at 0.33 and 0.61 GHz, and VLA observations between 5 and 22 GHz, of subkiloparsec scale radio emission from Mrk 231. In addition to jet components clearly associated with the AGN, we also find a smooth extended component of size 100 – 1000 pc most probably related to the purported massive star forming disk in Mrk 231. The diffuse radio emission from the disk is found to have a steep spectrum at high frequencies, characteristic of optically thin synchrotron emission. The required relativistic particle density in the disk can be produced by a star formation rate of $220 \text{ M}_{\odot} \text{ yr}^{-1}$ in the central kiloparsec. At low frequencies the disk is absorbed, most likely by ionized gas with an emission measure of $8 \times 10^5 \text{ pc cm}^{-6}$. We have also identified 4 candidate radio supernovae that, if confirmed, represent direct evidence for ongoing star formation in the central kiloparsec.

Subject headings: galaxies:active — galaxies:individual(Mrk 231) — galaxies: jets — galaxies:ISM — galaxies: nuclei — galaxies:halos

1. Introduction

Mrk 231 is one of the most luminous infrared galaxies in the local ($z < 0.1$) universe (Surace et al. 1998). As such it is potentially a key object for understanding the mechanism(s) that power such extreme far infrared dust emission. The most likely dust heating mechanisms are either (1) radiation from an AGN; or (2) a powerful starburst. The existence of an AGN in Mrk 231 is clearly demonstrated by the presence of a parsec-scale jet (Neff & Ulvestad 1988, Ulvestad, Wrobel, & Carilli 1999a), but the extent to which the AGN powers the high infrared luminosity ($10^{12} \text{ L}_{\odot}$) is unclear. Based on CO observations, Downes & Solomon (1998) suggest that most of the FIR luminosity in the central kpc of Mrk 231 comes from a starburst. Other evidence for

a starburst is the large amount of dust and extinction (Cutri, Rieke, & Lebofsky 1984). Based on its asymmetrical optical morphology with tidal tails, a merger in the last 10^9 years is likely (Hamilton & Keel 1987; Hutchings & Neff 1987; Armus et al. 1994; Surace et al. 1998). Even if the merger is not a direct energy source for the high infrared luminosity, it may play a critical role in channeling large amounts of gas and dust into the central kiloparsec, which then either feed the AGN or trigger the starburst.

Carilli, Wrobel, & Ulvestad (1998) report the discovery of a subkiloparsec scale disk seen in both the centimeter radio continuum and in neutral atomic hydrogen. Such a structure is almost unknown among AGN. Only one other radio source, 3C 84, has a ~ 100 pc disk or millihalo surrounding the parsec-scale jets (Silver, Taylor, & Vermeulen 1998). In the case of 3C 84, the most likely origin for the millihalo is from relativistic particles that have diffused out from the parsec-scale jets, but a starburst origin cannot be completely ruled out. Carilli et al. suggested that the millihalo seen around Mrk 231 is really a disk with a massive star formation rate of order $100 M_{\odot} \text{ yr}^{-1}$. Here we present further VLBA observations of the disk in Mrk 231 at 0.61 and 0.33 GHz in an attempt to learn more about its spectrum and structure. We have also reduced and analyzed archival VLA observations which reveal the outer part of the disk at 5 – 22 GHz.

We assume $H_0 = 50 \text{ km s}^{-1} \text{ Mpc}^{-1}$ and $q_0 = 0.5$ throughout, so at the redshift of Mrk 231 of 0.04152 (de Vaucouleurs et al. 1991), $1''$ corresponds to 1.12 kpc.

2. VLBA Observations and Data Reduction

The VLBA observations were carried out at 0.333 and 0.613 GHz with the 10-element VLBA of the NRAO¹ in a single 10-hour observing session on 1998 June 20. The net integration time on Mrk 231 was 250 minutes at each frequency spread over multiple snapshots to improve u, v coverage. Both frequencies were observed simultaneously with 3 IF bands covering the frequency range 0.328–0.340 GHz and 1 IF covering the range 0.611–0.615 GHz. Both right- and left-circular polarizations were observed with 2-bit sampling. Due to strong external interference near 0.613 GHz a 3.4 MHz passband filter was used on all antennas. The correlator produced a 2.06 second integration time and 16 channels per IF band.

Standard *a priori* flagging, amplitude calibration, fringe fitting, bandpass calibration, and frequency averaging procedures were followed in AIPS. Phase referencing was performed by correlating at the position of the quasar J1252+5634 located some $36'$ from Mrk 231. Global fringe fitting was performed on J1252+5634 and the resulting delays, rates and phases transferred to Mrk 231. Subsequently, Mrk 231 was phase-only self-calibrated with a 2 minute solution interval. All manual editing, imaging, deconvolution, and self-calibration were performed using DIFMAP

¹The National Radio Astronomy Observatory is operated by Associated Universities, Inc., under cooperative agreement with the National Science Foundation

(Shepherd, Pearson, & Taylor 1994; Shepherd 1997).

In Fig. 1 we show the 0.33 GHz and 0.61 GHz VLBA images at a resolution of 30 mas. Both images are dominated by a compact source, just resolved in the north-south direction. Due primarily to the greater bandwidth, the 0.33 GHz image is more sensitive by a factor of ~ 2 .

We have also reanalyzed the 1.36 GHz continuum data of Carilli et al. (1998). By performing careful editing and self-calibration within DIFMAP we were able to achieve an image with a rms noise of 0.02 mJy/beam (Fig. 2). The Pie Town – VLA baseline was removed, eliminating the extended inner disk emissions which are not easily deconvolved and otherwise severely limit the achievable dynamic range.

3. VLA Observations and Data Reduction

All the VLA observations reported here are A configuration observations retrieved in raw form from the VLA archive. These observations were carried out using the VLA in the standard fashion with a 100 MHz continuum observing mode at 4.86, 8.44, 14.94 and 22.23 GHz at epoch 1995.55, 1991.48, 1983.87, and 1996.99 respectively. The total observing time on Mrk 231 was 210, 15, 35, and 90 minutes at 5–22 GHz respectively.

Once the data were calibrated in AIPS, they were exported to DIFMAP for further self-calibration. To better reveal the underlying extended emission, a delta function was subtracted from the phase center of each observation. The resulting naturally weighted images are shown in Fig. 3. The amplitude of the delta function subtracted represents the emission from the VLBI triple seen on scales of ~ 40 mas (Ulvestad et al. 1999a), and the 30 – 100 mas radius inner disk component first detected by Carilli et al. (1998). This sum is labeled the “nucleus” in Table 1 and in Fig. 4. The remaining flux density in the images (radii of 0.1 – 1”), is labeled the “outer disk” in Table 1.

TABLE 1
COMPONENT FLUX DENSITIES AND SPECTRA

Component	S_{22} (mJy)	S_{15} (mJy)	$S_{8.4}$ (mJy)	S_5 (mJy)	$S_{1.3}$ (mJy)	$S_{0.61}$ (mJy)	$S_{0.33}$ (mJy)
C+N+S+ID	59±9	110±11	208±15	269±14	230±12	–	–
C+N+S	–	62±6	142±14	173±17	99±10	163±16	152±15
S. Jet	–	–	–	–	–	28±3	44±4
Inner Disk	–	48±5	66±7	96±10	131±13	–	30±6
Outer Disk	13.1±0.7	25.3±1.3	32.7±1.7	25.9±1.3	–	–	–

4. The Jet Components

The dominant “core” component in our VLBA images is really comprised of a north-south triple (Ulvestad et al. 1999a). This triple includes a GHz peaked spectrum core between two steep spectrum lobes with the southern lobe being the brighter of the two. The total extent is about 60 mas (70 pc). This structure is just resolved in our 0.61 and 0.33 GHz images. At 1.3 GHz, the spectra of parts of the N and S lobes are turning over, while the spectrum of the core turns over near 8 GHz (Ulvestad et al. 1999a). As these are the dominant components, on that basis one might have expected very little flux density at 0.33 GHz. We see from our Fig. 4 that the spectrum of the core conglomerate (N+C+S at this resolution of 30 mas) is essentially flat out to 0.33 GHz. This may be due in part to a steep spectrum contribution from the jet that connects both lobes to the core hinted at in Fig. 1a of Ulvestad et al. The absence of dominant free-free opacity indicates that at least some parts of the nuclear region have a relatively unobstructed line-of-sight to the observer, perhaps cleared out by the AGN.

A new component is seen in our VLBA images some 107 mas south of the core in position angle 171° . This component is curved into a bowshock-like structure similar in appearance to the southern (S) component of the VLBI triple at 2.3 GHz (see Fig. 3 of Ulvestad et al. 1999a). Based on its location along the jet axis, we identify this component as part of the southern jet. The spectral index between 0.61 and 0.33 GHz of this new southern jet component is steep ($\alpha = -0.74 \pm 0.2$ where $S_\nu \propto \nu^\alpha$) as would be expected for such a large (80 mas FWHM) emission region. This component is also detected at 1.36 GHz (Fig. 2) as a group of subcomponents – the broken-up appearance is probably due to a lack of sufficiently short baselines at this frequency to adequately sample this large component. Furthermore the fact that this component is most likely unaffected by the free-free absorption suspected towards the inner disk (see below), indicates that the line-of-sight towards this component is relatively unobstructed. One possibility is that this jet component is on the approaching side in front of the disk, consistent with the schematic view put forth by Carilli et al. (1998). The smallest scale VLBI structure appears to be a one-sided sub-relativistic jet pointing to the southwest. The one-sided appearance is probably due to free-free absorption on sub-parsec scales (Ulvestad et al. 1999b); this supports the argument that the southwestern jet imaged by Ulvestad et al. (1999a) is in front of the disk and leads into the more extended southern VLBI lobe.

5. Properties of the Disk in MRK 231

5.1. Diffuse Radio Emission

Diffuse, extended emission on scales of ~ 1 kpc is seen in a number of Seyfert galaxies (Wilson 1988, Ulvestad & Wilson 1989). In fact, based on observations with the partially completed VLA in 1979, Ulvestad, Wilson & Sramek (1981) presented evidence of 10–15 mJy of extended emission

around Mrk 231 at 4.9 GHz, though this emission was not well localized by those observations. In Fig. 3, we present higher resolution observations at 5 – 22 GHz that clearly show extended emission in a fairly circular disk centered on the nucleus. The radial fall-off beyond 200 mas is Gaussian with a FWHM of 860 mas (980 pc) (Fig. 5). At all frequencies a north-south extension is visible in the inner contours. At lower flux density levels the disk appears nearly circular, with a possible extension to the East.

The existence of a subkiloparsec gas (and stellar?) disk in Mrk 231 is now well documented through high resolution molecular line observations (Bryant & Scoville 1996, Downes & Solomon 1998), H I 21cm absorption line observations, and radio continuum observations (Carilli et al. 1998). For illustration, we reproduce the results of the H I 21cm absorption line observations in Fig. 6. This figure shows the position-velocity diagram along the major axis (oriented east-west) of the inner disk for H I 21cm absorption. Note the clear velocity gradient of $\pm 130 \text{ km s}^{-1}$ to radii $\approx 200 \text{ mas}$. The peak H I optical depth is 0.17. It is likely that the H I extends farther than is observed in Fig. 6. The spatial limit is set by the surface brightness of the diffuse radio continuum emission against which the absorption is seen. The CO disk seen by Bryant & Scoville (1996) on a factor ~ 3 larger scale has the same velocity gradient and position angle of the major axis. Carilli et al. (1998) show that the diffuse radio continuum emission seen on scales from 100 mas to 1 arcsecond in Mrk 231 is likely to be associated with this gas disk, and in particular with massive star formation. We consider this hypothesis further below.

The radio continuum images presented herein reveal the structure of the disk at frequencies ranging from 0.33 GHz to 22 GHz. The size of the disk at 5 GHz (Fig. 3) is $1.9'' \times 1.6''$ to the 5σ surface brightness level of $0.16 \text{ mJy beam}^{-1}$. The position angle of the major axis is $\sim 55^\circ$. For comparison, the disk seen in CO emission has a Gaussian FWHM = $0.9'' \times 0.8''$ at a position angle of 77° . Downes & Solomon (1998) fit gas kinematic models to the CO velocity distribution and find a disk thickness of 23 pc. Both the radio continuum and CO data imply that the disk must be close to face-on, with $i \approx 30^\circ$.

The spectral index of the radio continuum outer disk emission between 5 GHz and 8 GHz is -0.7 ± 0.2 for radii between $0.4''$ and $0.7''$. This is consistent with non-thermal synchrotron emission from a population of relativistic electrons accelerated in shocks driven by supernova remnants, as would be the case for active star formation in the disk (Condon 1992). The IR-to-radio flux density ratio parameter, Q , for the disk is 2.5 (Carilli et al. 1998). This value is consistent with the value of $Q = 2.3 \pm 0.2$ seen for the integrated emission from starforming galaxies (Condon 1992). The flux density of the disk at 1.3 GHz is 130 mJy, implying a radio spectral luminosity of $9 \times 10^{30} \text{ ergs s}^{-1} \text{ Hz}^{-1}$. Using the empirical relations in Condon (1992) leads to a massive star formation rate in the disk of $220 \text{ M}_\odot \text{ yr}^{-1}$, and an expected supernova rate of 8 yr^{-1} .

An important question is: do the synchrotron emitting electrons originate in the disk, or are they somehow transported to the disk from the AGN region? One key factor to consider is the timescale for relativistic electron transport compared to the lifetimes of the relativistic electrons

due to synchrotron and inverse Compton losses. For fields of order 200 μG (see below), the expected lifetime of the particles radiating at 5 GHz is of order 10^5 yrs. A standard assumption in ISM plasma physics is that the cosmic ray electrons are limited to stream at the Alfvén velocity due to scattering off self-induced Alfvén waves – the streaming energy is converted into hydromagnetic waves by the two-stream instability (Wentzel 1974). Using a thermal particle density of 185 cm^{-3} (see below) implies an Alfvén speed of 15 km s^{-1} in the disk, or a propagation length of only 1.5 pc in 10^5 yrs. This short distance would argue in favor of *in situ* particle acceleration in the disk. On the other hand, high energy electrons originating in solar flares are known to propagate hyper-Alfvénically in the inter-planetary medium, in violation of the standard theory (Hudson & Ryan 1995). The other extreme is to assume that all the particles stream at the velocity of light, c , along a tangled magnetic field. The timescale, t_o , for the particles to ‘random walk’ a distance R_o becomes: $t_o \approx \frac{R_o^2}{l_o c}$, where l_o is the cell size for the turbulent field. Using $R_o \approx 1'' = 1120\text{ pc}$ (= maximum observed radius of the disk at 5 GHz), leads to: $t_o \approx 1 \times 10^5 [\frac{l_o}{40\text{ pc}}]^{-1}$ yrs. Hence, if the turbulent magnetic field cell size is greater than 40 pc, and if the particles are somehow allowed to stream at the speed of light, then it is possible that the diffuse radio continuum emitting regions in Mrk 231 could be populated by electrons from the active nucleus.

Other arguments in favor of *in situ* particle acceleration in the disk are: (i) the observed distribution (position angle of major axis, and major-to-minor axis ratio) of the radio continuum emission is similar to that seen for the CO disk, (ii) the spectral index of the extended AGN components between 2.3 GHz and 8.4 GHz is -1.5 (Ulvestad et al. 1999a), which is considerably steeper than is seen for the disk, (iii) the disk emission obeys the IR-radio correlation for star forming galaxies, and (iv) physical conditions in the disk are conducive to star formation, and the star formation rate derived from the molecular line observations is comparable to that derived from the radio continuum observations (Downes & Solomon 1998, Bryant & Scoville 1996). Overall, we feel it is most likely that the diffuse radio continuum emission is driven by star formation in the disk, although we cannot rule-out an AGN origin for the relativistic electrons.

5.2. Free-free absorption of the inner disk

The integrated spectrum of the inner disk ($\leq 100\text{ mas}$) in Mrk 231 shows an inversion below 1.3 GHz, most likely due to free-free absorption (Fig. 4). We have fit a free-free absorption model to the data, and obtain an emission measure, $\text{EM} = 7.9 \pm 0.6 \times 10^5 (\frac{T_K}{10^4})^{\frac{3}{2}}\text{ pc cm}^{-6}$, where T_K is the kinetic temperature of the gas. Using a disk thickness of 23 pc leads to $n_e = 185 (\frac{T_K}{10^4})^{\frac{3}{4}}\text{ cm}^{-3}$ and $N_e = 1.3 \times 10^{22} (\frac{T_K}{10^4})^{\frac{3}{4}}\text{ cm}^{-2}$. This column density is comparable to the hydrogen column density derived from CO observations (Downes & Solomon 1998), in H I assuming a spin temperature of 1000 K (Carilli et al. 1998), and to the hydrogen column density inferred from soft X-ray absorption of $6 \times 10^{22}\text{ cm}^{-2}$ (Nakagawa et al. 1997).

The pressure in the ionized absorbing medium is $5 \times 10^{-10} (\frac{T_K}{10^4})^{\frac{7}{4}}\text{ dynes cm}^{-2}$. The pressure

in the molecular gas in the disk is $5 \times 10^{-11}/f$ dynes cm^{-2} , where f is the volume filling factor. Hence, pressures in the ionized and molecular components are comparable assuming a reasonable filling factor of 0.1 for the molecular gas (Downes & Solomon 1998). The minimum pressure in the relativistic electrons and magnetic fields ranges from 2×10^{-10} dynes cm^{-2} in the outer disk to 10×10^{-10} dynes cm^{-2} in the inner disk, making the standard assumptions of Miley (1980), and in particular using a low value for the proton-to-electron energy density ratio, ($k \approx 1$) and assuming unit filling factor. The corresponding magnetic field strengths are 80 μG and 200 μG , respectively.

5.3. Candidate Radio Supernovae

A final question that can be addressed by these data is the existence of radio supernovae (RSNe) in the disk of Mrk 231. Recent VLBI observations of Arp 220 have revealed 13 RSNe in the inner 100 pc with flux densities at 1.3 GHz between 0.1 and 1.2 mJy, with three RSNe between 1.0 mJy and 1.2 mJy (Smith et al. 1998). Smith et al. show that these RSNe are of the same class as RSN 1986J observed in the disk of NGC 891 (Rupen et al. 1987): Type II RSNe with luminosities of order 10^{28} ergs s^{-1} Hz^{-1} and exponential decay times of 3 yrs. The number of RSNe observed in Arp 220 is consistent with a massive star formation rate of 70 M_{\odot} yr^{-1} .

We have searched for RSNe in Mrk 231 at a resolution of 10 mas at 1.3 GHz (Fig. 2). The difficulty in Mrk 231 is confusion of the inner 50 pc due to the AGN radio components. Based on the observations of Arp 220, and correcting for the relative distances, the predicted number of RSNe ≥ 0.2 mJy in Mrk 231 is six. We have identified four possible RSNe candidates between 0.2 and 0.5 mJy that are not along the jet or counterjet axis. The brightest of these four (source A) is certainly a real source, but it is close to the radio axis and hence may be related to the AGN. The fainter sources (B,C,D) are farther away from the radio axis, and are detected at the $\sim 10\sigma$ level, but we cannot rule out that these ‘sources’ are imaging artifacts caused by dynamic range limitations imposed by the presence of the strong AGN components. The arc of star-forming knots $\sim 3''$ south of the core (on the radio-jet axis) seen by Surace et al. (1998) may be jet-induced. While it is possible that the jet may trigger star formation along the radio axis closer to the nucleus, we cannot from our radio observations alone distinguish such emission from jet emission related to the AGN. The RSNe in Mrk 231 hypothesis could be tested by monitoring the system with annual, sensitive, high quality VLBI imaging to determine the light curves for the faint possible sources in the star forming disk.

We are grateful to Joan Wrobel, and the referee, J. Mazzarella, for insightful comments. This research has made use of the NASA/IPAC Extragalactic Database (NED) which is operated by the Jet Propulsion Laboratory, Caltech, under contract with NASA.

REFERENCES

- Armus, L., Surace, J. A., Soifer, B. T., Matthews, K., Graham, J. R., & Larkin, J. E. 1994, *AJ*, 108, 76
- Bryant, P. M., & Scoville, N. Z. 1996, *ApJ*, 457, 678
- Carilli, C. L., Wrobel, J. M., & Ulvestad, J. S. 1998, *AJ*, 115, 928
- Condon, J. J. 1992, *ARA&A*, 30, 575
- Cutri, R. M., Rieke, G. M., & Lebofsky, M. J. 1984, *ApJ*, 287, 566
- de Vaucouleurs, G., de Vaucouleurs, A., Corwin, H. G., Jr., Buta, R. J., Paturel, G., & Fouqué, P. 1991, *Third Reference Catalogue of Bright Galaxies* (New York: Springer)
- Douglas, J. N., Bash, F. N., Bozyan, F. A., Torrence, G. W., & Wolfe, C. 1996, *AJ*, 111, 1945
- Downes, D., & Solomon, P. M. 1998, *ApJ*, 507, 615
- Hamilton, D., & Keel, W. C. 1987, *ApJ*, 321, 211
- Hudson, H., & Ryan, J. 1995, *ARA&A*, 33, 239
- Hutchings, J. B., & Neff, S. G. 1987, *AJ*, 93, 14
- Miley, G. K. 1980, *ARA&A*, 18, 165
- Nakagawa, T., Kii, T., Fujimoto, R., Miyazaki, T., Inoue, H., Ogasaka, Y., Arnaud, K., & Kawabe, R. 1997, *IAU Symposium 186, Galaxy Interactions at Low and High Redshift*, p. 103
- Neff, S. G., & Ulvestad, J. S. 1988, *AJ*, 96, 841
- Rupen, M. P., van Gorkom, J. H., Knapp, G. R., Gunn, J. E., & Schneider, D. P. 1987, *AJ*, 94, 61
- Shepherd, M. C., Pearson, T. J., & Taylor, G. B. 1994, *BAAS*, 26, 987
- Shepherd, M. C. 1997, *Astronomical Data Analysis Software and Systems VI*, eds. G. Hunt & H. E. Payne (San Francisco: ASP), 77
- Silver, C. S., Taylor, G. B., & Vermeulen, R. C. 1998, *ApJ*, 502, 229
- Smith, H. E., Lonsdale, C. J., Lonsdale, C. J., & Diamond, P. J. 1998, *ApJ*, 493, L17
- Surace, J. A., Sanders, D. B., Vacca, W. D., Veilleux, S., & Mazzarella, J. M. 1998, *ApJ*, 492, 116
- Ulvestad, J. S., Wilson, A. S., & Sramek, R. A. 1981, *ApJ*, 247, 419
- Ulvestad, J. S., & Wilson, A. S. 1989, *ApJ*, 343, 659
- Ulvestad, J. S., Wrobel, J. M., & Carilli, C. L. 1999a, *ApJ*, in press
- Ulvestad, J. S. et al. 1999b, *ApJL*, in preparation
- Wentzel, D. G. 1974, *ARA&A*, 12, 71
- Wilson, A. S. 1988, *A&A*, 206, 41

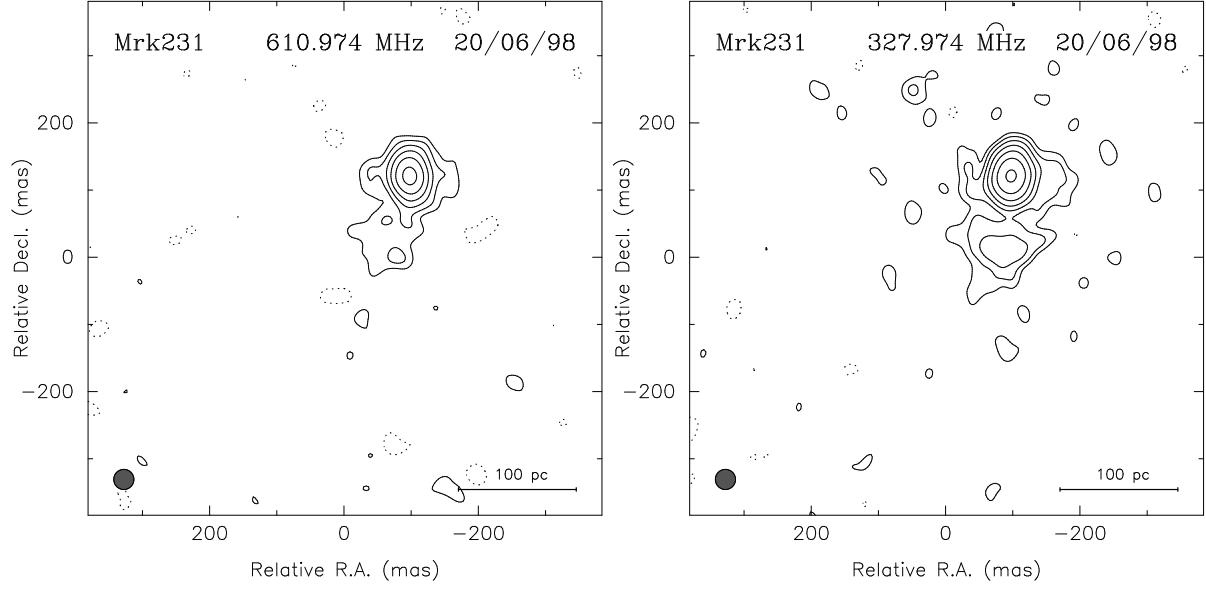


Fig. 1.— The naturally weighted and tapered images of Mrk231 at 0.61 and 0.33 GHz. The resolution of both images is 30 mas. Contours are at factor 2 intervals and start at 2 and 1 mJy/beam for 0.61 and 0.33 GHz respectively.

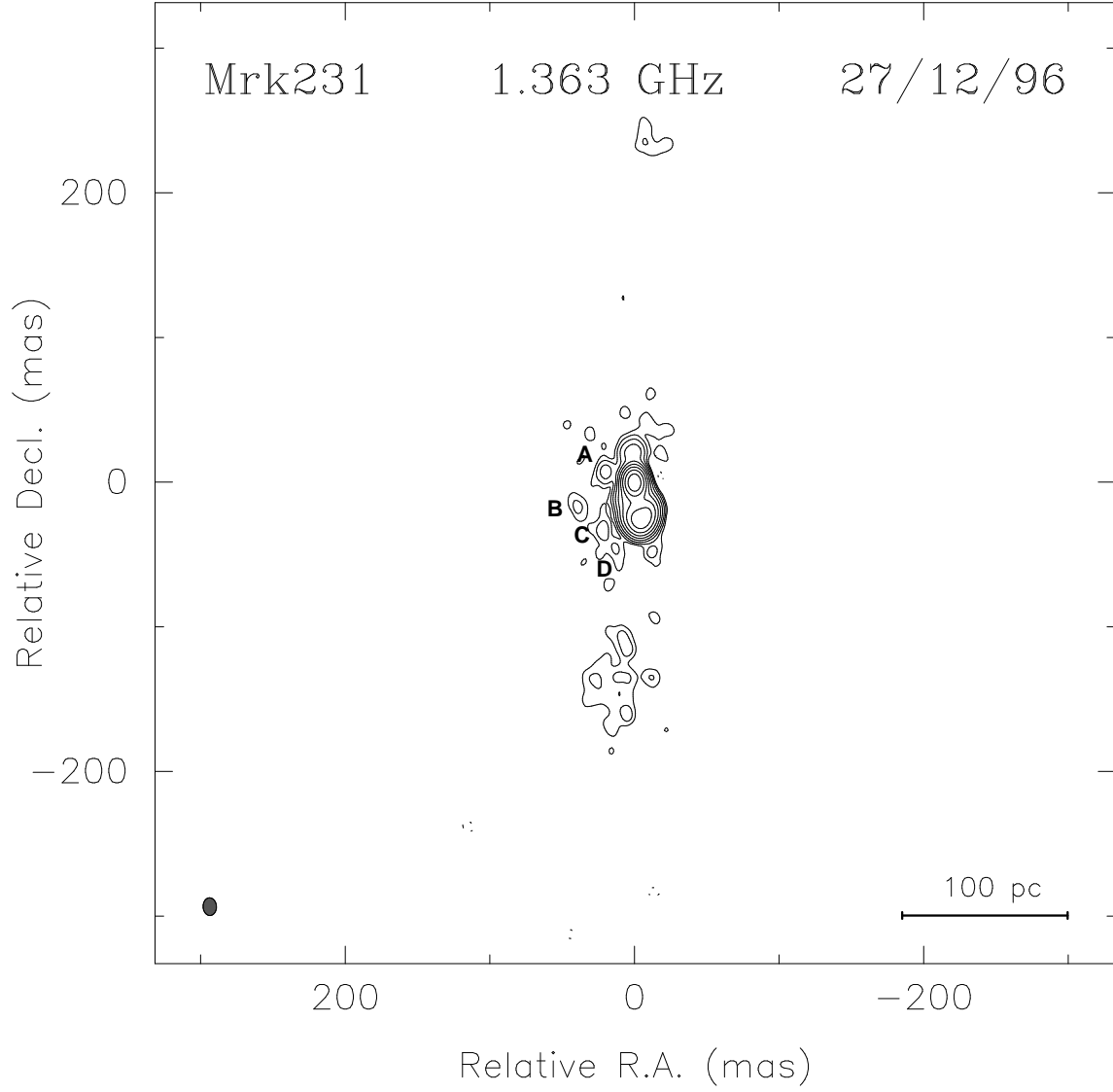


Fig. 2.— The 1.3 GHz continuum data of Carilli et al. (1998) reimaged with a naturally weighted beam of 12.3×9.3 mas in p.a. 3° . Contours are drawn at factor 2 intervals and start at 0.1 mJy/beam (5σ). Four RSNe candidates are labeled A–D.

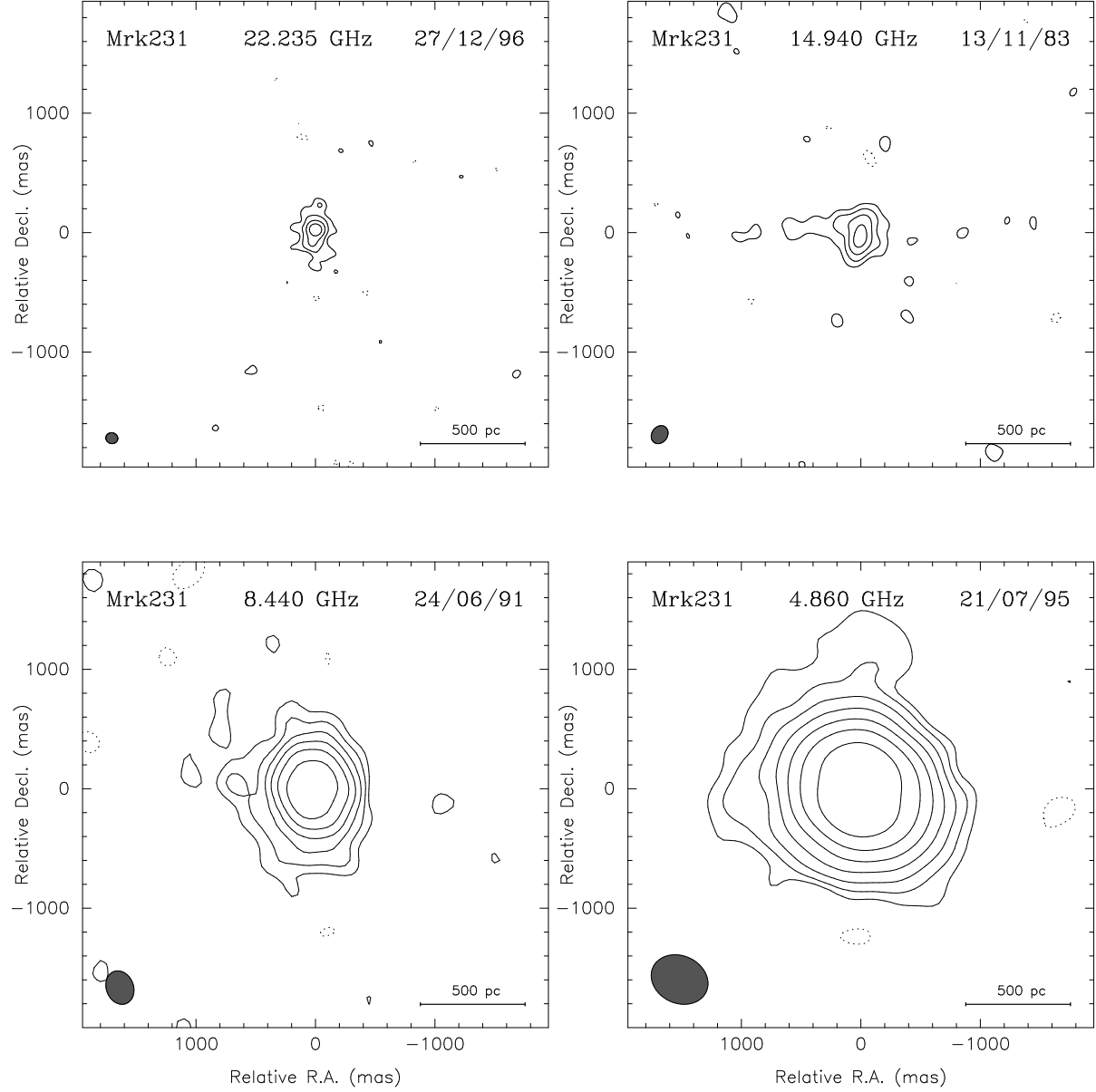


Fig. 3.— VLA images of Mrk 231 at 22, 15, 8 and 5 GHz. A delta function has been removed before imaging as described in the text. The beam shapes are shown in the lower left corner. Contours are at factor 2 intervals and start at 0.5, 0.8, 0.12 and 0.08 mJy/beam for 22, 15, 8 and 5 GHz respectively.

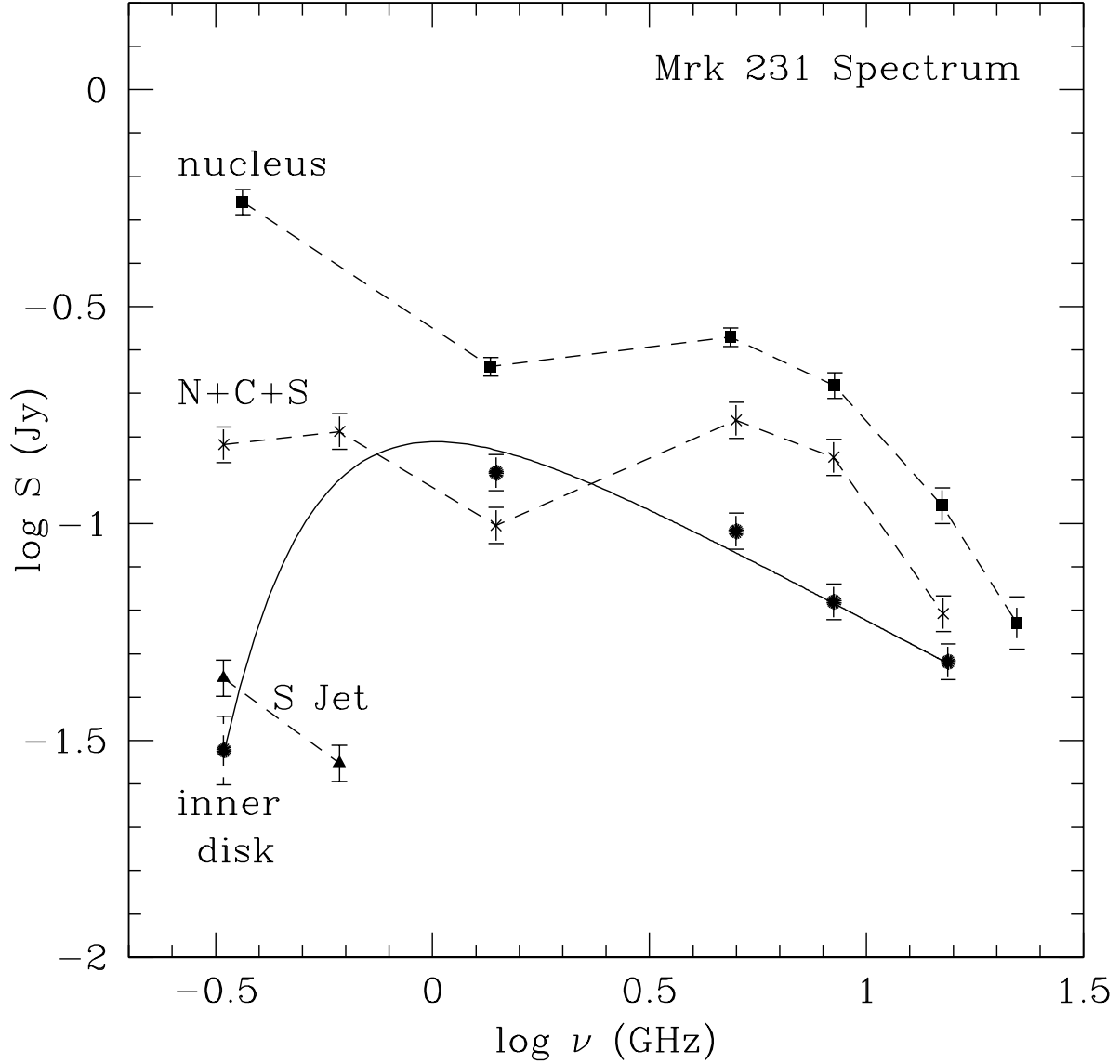


Fig. 4.— The spectrum of the constituent components of Mrk 231 on subkiloparsec scales. The nucleus (squares) refers to the VLA core which is presumed to be the sum of the VLBI triple (N+C+S – crosses) and the disk (filled circles). The triangles denote measurements of a newly detected southern jet component. Measurements of these components come from Ulvestad et al. (1999) and this paper, except for the flux density of the nucleus at 0.365 GHz, which is from Douglas et al. (1996). A free-free absorption model (solid line) is fit to the disk emission as discussed in the text.

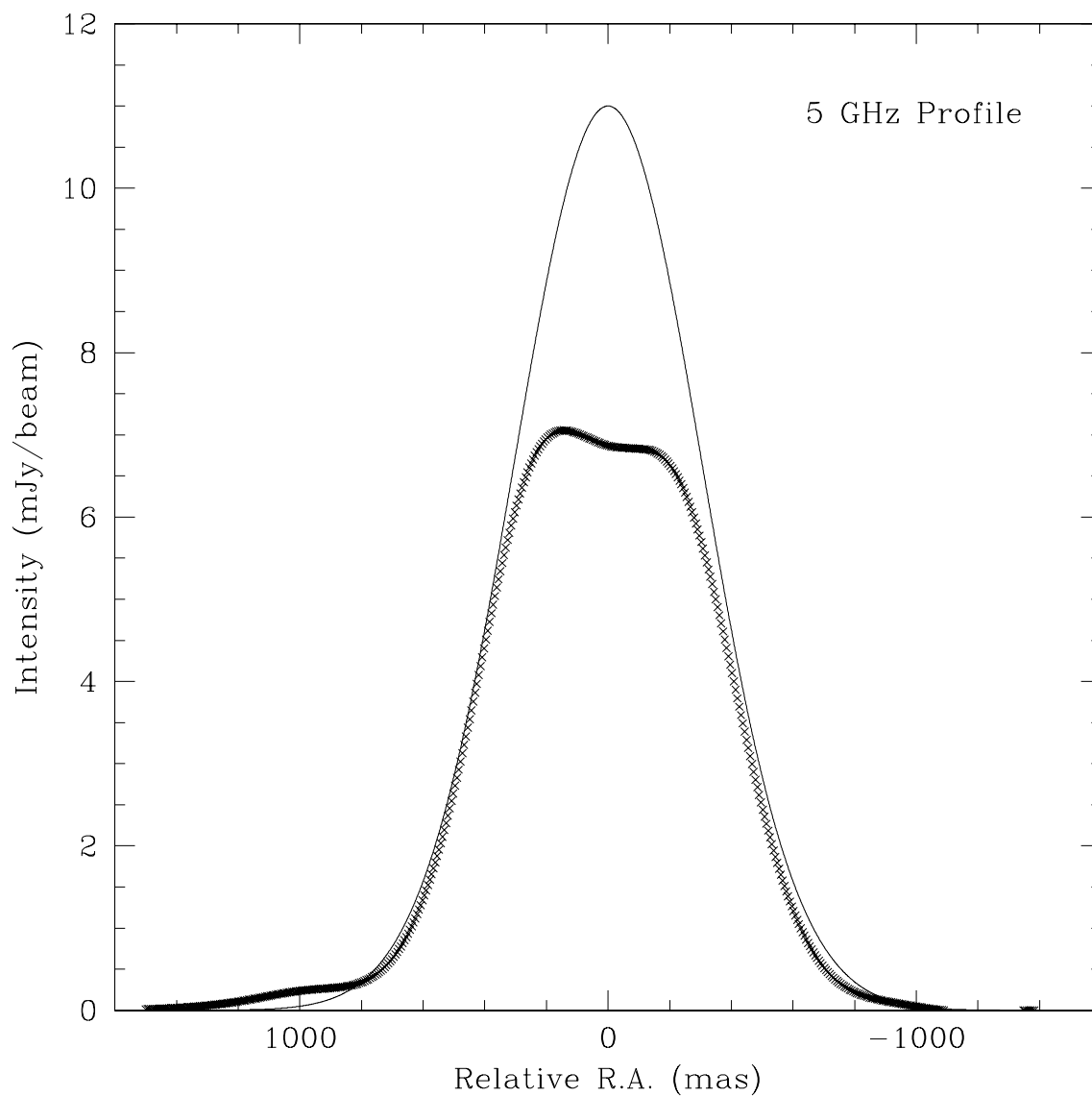


Fig. 5.— An east-west slice through the 5 GHz image of the outer disk shown in Fig. 3. The solid line indicates a Gaussian fit with FWHM 860 mas.

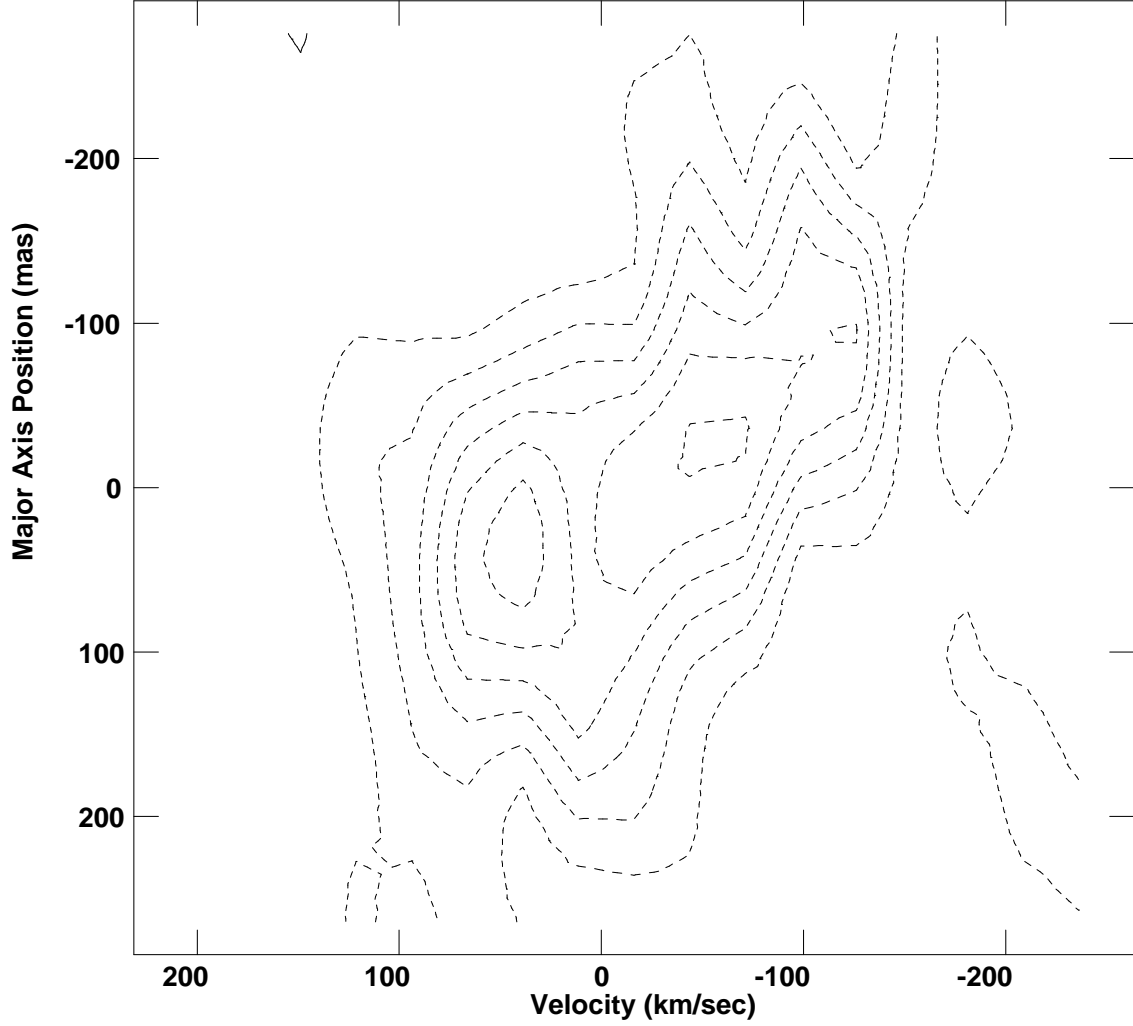


Fig. 6.— The HI position-velocity diagram for Mrk 231 along the major axis of the disk in position angle 90° . Contours are drawn at $-6, -5, -4, -3, -2, -1$, and 1 mJy/beam. The beam has a FWHM of 150 mas. The peak optical depth is 0.17 , and zero velocity corresponds to a heliocentric redshift of 0.04217 ($cz = 12642$ km s $^{-1}$). The velocity resolution is 56 km s $^{-1}$.